Supporting Information

Eutectic Electrolyte Enables the Reversible Zn Electrodeposition Based Electrochromic Devices with Large Optical Modulation and Robust Cycling Stability

Yu Zhong, Ying Du, Xiaodan Guo, Jinhui Wang, Guofa Cai*

[a] Key Laboratory for Special Functional Materials of Ministry of Education, National & Local Joint Engineering Research Center for High-Efficiency Display and Lighting Technology, School of Nanoscience and Materials Engineering, Henan University, Kaifeng 475004, China.

*Corresponding author: caiguofa@henu.edu.cn (Guofa Cai).

Experimentation section

Synthesis of DES Electrolytes

All chemicals and reagents were of analytical grade and used without further purification. Ethylene glycol (EG), choline chloride (ChCl), and anhydrous zinc chloride ($ZnCl_2$) were purchased from Greagent, Adamas, and Macklin, respectively. A homogeneous and transparent DES was prepared by mixing ChCl and EG in a molar ratio of 1:2, followed by stirring at 80 °C for 1 h. Then, electrolytes with concentrations of 0.1, 0.2, 0.3, 0.4, 0.5, 0.6 and 0.7 M $ZnCl_2$ were prepared, referred to as DES1, DES2, DES3, DES4, DES5, DES6 and DES7, respectively. The upper solubility limit of $ZnCl_2$ in DES is 0.5 M at room temperature (Figure S1 and S2), so the concentration range of subsequent studies is 0.1~0.5 M.

Assembly of RME Electrochromic Device

The RME electrochromic device was assembled using fluorine-doped tin oxide-coated (FTO) glass as the working electrode, Zn frame as the counter electrode and DES as the electrolyte. Prior to assembly, the FTO glass was ultrasonically cleaned with acetone, deionized water (DI) and ethanol for 15 min each. To assemble the device, the FTO and Zn frame along with a non-conducting piece of glass, were spatially separated using double-sided adhesive tape (VHB4010, 3 M). After that, the prepared DES electrolyte was slowly injected between the two electrodes and then encapsulated with epoxy resin adhesive to prevent electrolyte leakage. Finally, the RME electrochromic device was obtained.

Electrochemical and Electrochromic Characterization

All electrochemical measurements were performed using a PARSTAT MC electrochemical workstation. Cyclic voltammetry (CV), chronoamperometry (CA) and galvanostatic charge/discharge (GCD) of various DESs were conducted in a three-electrode system. Bare FTO, Zn foil and Pt wire were used as the working, reference and counter electrode, respectively. Zn film deposition/dissolution were conducted using a two-electrode system, with FTO as the working electrode and Zn frame as the counter electrode. In situ electrochromic measurements were carried out in a spectroelectrochemical cell by combination of an ultraviolet-visible-infrared (UV-VIS-NIR) spectrophotometer (SHIMADZU SolidSpec-3700i) and an electrochemical workstation.

Characterization

The viscosity and density of various DES were measured using a DMA 4100 M. The ionic conductivity of electrolytes at different temperatures was measured using a DDSJ-308F. The composition and morphology of the samples were analyzed by scanning electron microscopy (SEM, HITACHI SU8220), Raman microscopy (Renishaw inVia), X-ray photoelectron spectroscopy (XPS, Thermo SCIENTIFIC

ESCALAB 250Xi) and Fourier transform infrared spectroscopy (FTIR, PerkinElmer, Frontier IR/FIR STA 8000). The optical transmittance and reflectance spectra of the samples in response to different electrochemical stimulations were obtained using a UV-VIS-NIR spectrophotometer.

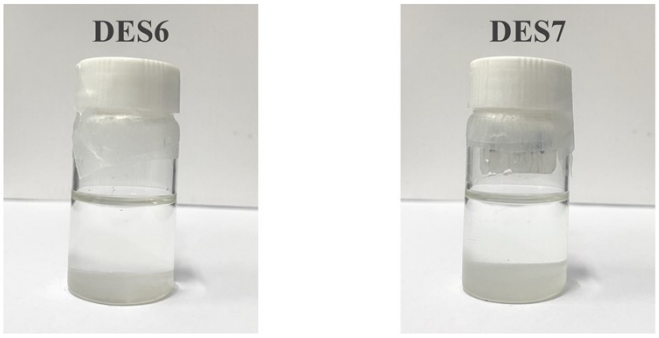

Figure S1. The optical photographs of DES6 and DES7 electrolytes at 25 °C.

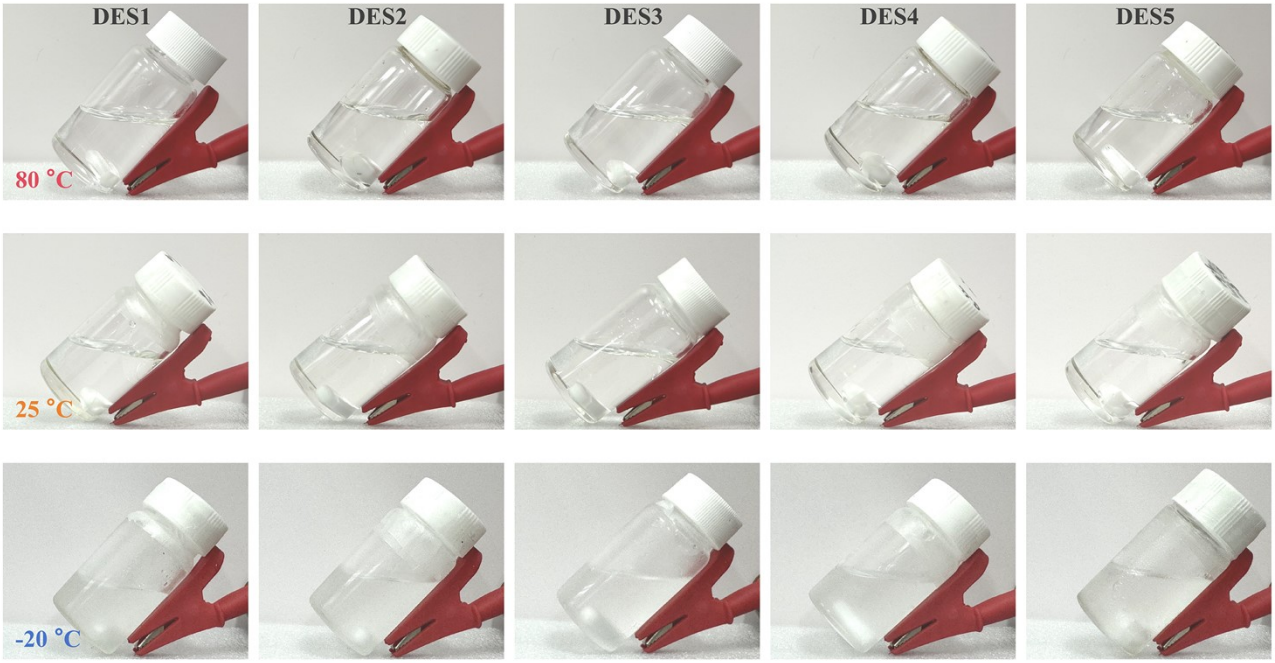

Figure S2. The optical photographs of different DES electrolytes at -20, 25 and 80 °C.

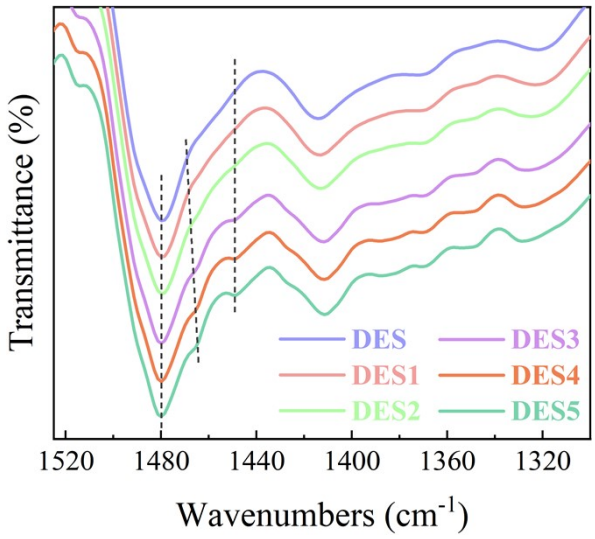

Figure S3. FTIR spectra of various DES electrolytes.

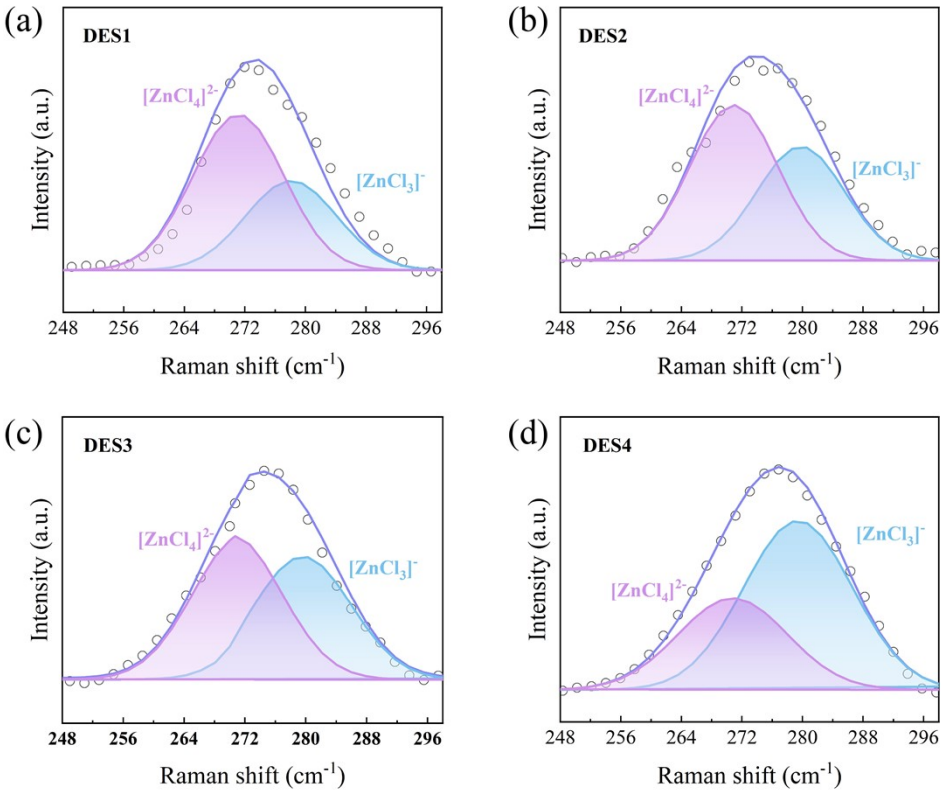

Figure S4. The fitting peaks of $[ZnCl_x]^{2-x}$ in DES1-4 electrolytes.

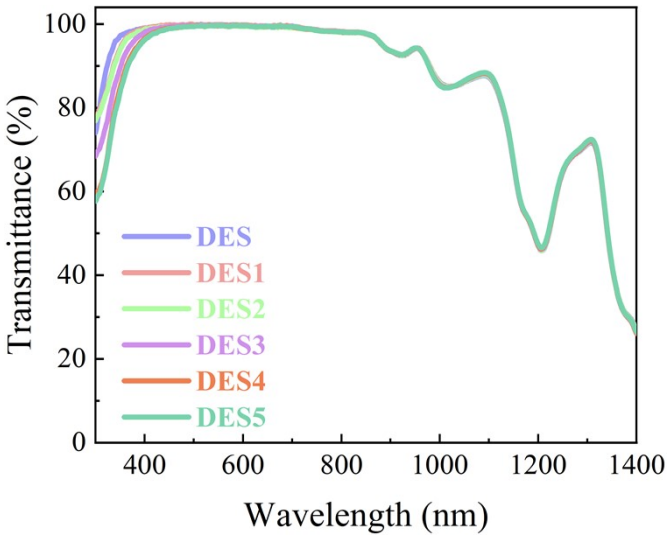

Figure S5. Transmittance spectrum (300-1400 nm) of different DES-based electrolytes at 25 °C.

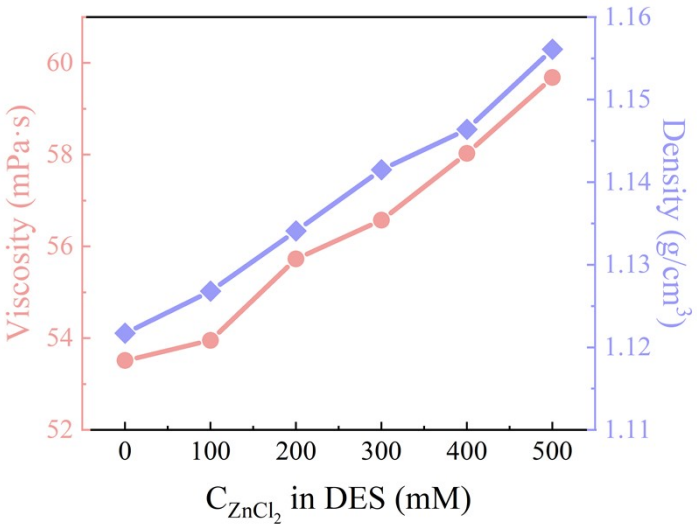

Figure S6. Viscosity and density of different $ZnCl_2$ concentration at 25 °C.

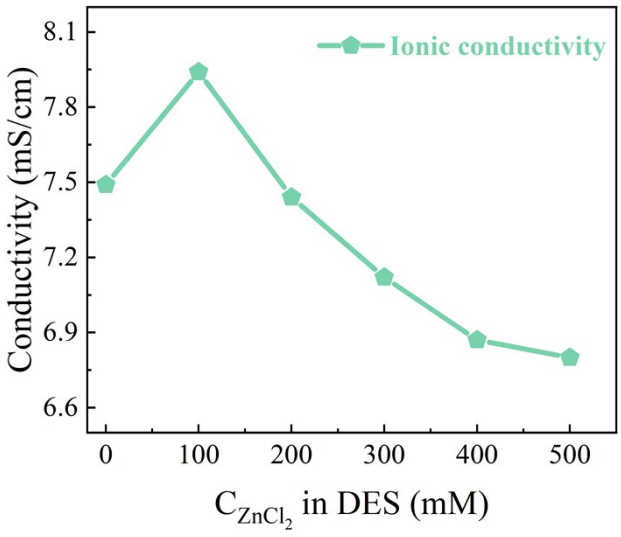

Figure S7. Ionic conductivity of various $ZnCl_2$ concentration at 25 °C.

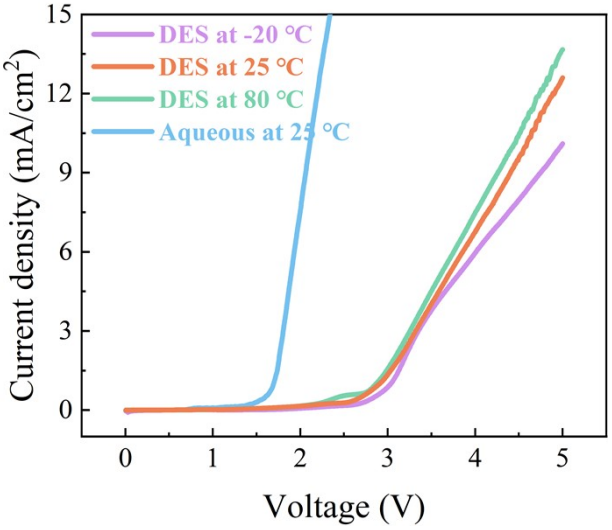

Figure S8. Electrochemical stability window of DES-based electrolyte and $ZnCl_2$ aqueous solution.

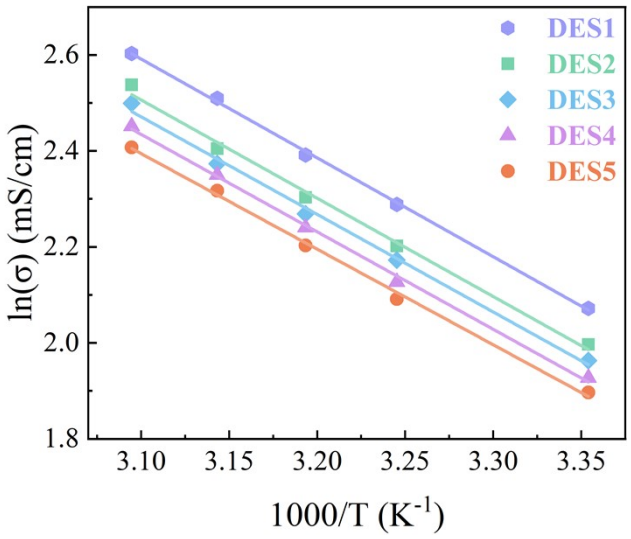

Figure S9. Temperature dependence of ionic conductivity in various DES electrolytes based on the Arrhenius equation.

The activation energy for Zn^{2+} migration was derived by fitting the temperature-dependent ionic conductivity data to the Arrhenius equation according to the following relationship:

$$\sigma = A\ exp(-\frac{E_a}{RT})$$

where σ is the ion conductivity, E_a is the activation energy for ion migration, A is the pre-exponential factor, R is the molar gas constant, T is the absolute temperature.

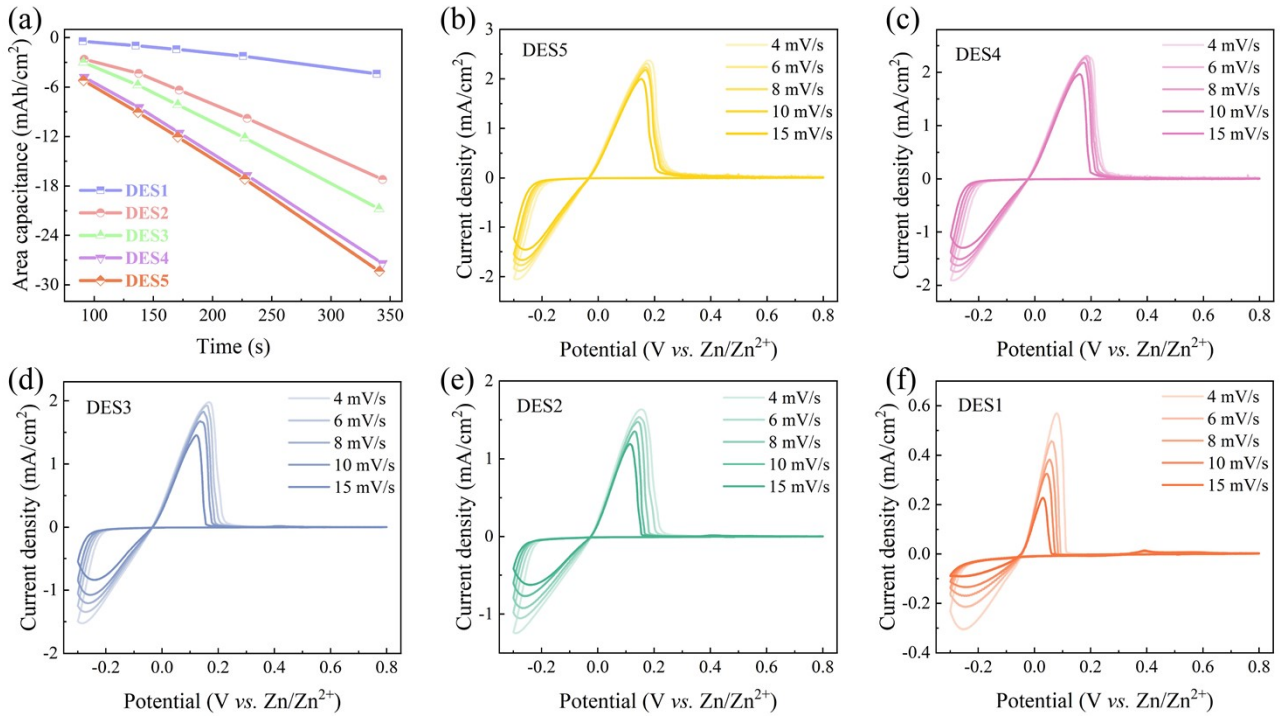

Figure S10. (a) The area capacitance in various DES-based electrolytes; (b-f) CV curves of the Zn plating and stripping behavior at different scan rates (from 4 to 15 mV/s) in DES1-5 electrolytes.

The ion transport flux of DES-based electrolytes can be calculated as the molar number of Zn^{2+} passing through unit area of electrode/electrolyte interface in an hour (mol/m^2/h) during charge/discharge reaction using following equation:

$$\emptyset_{Zn^{2+}} = \frac{10000 C_{area}}{C_{Zn} M_{Zn} t}$$

where $\emptyset_{Zn^{2+}}$ is the Zn^{2+} transport throughput, C_{area} is the area specific capacity, C_{Zn} is the theoretical specific capacity of Zn, M_{Zn} is the Molar mass of Zn, t is the charge/discharge time.

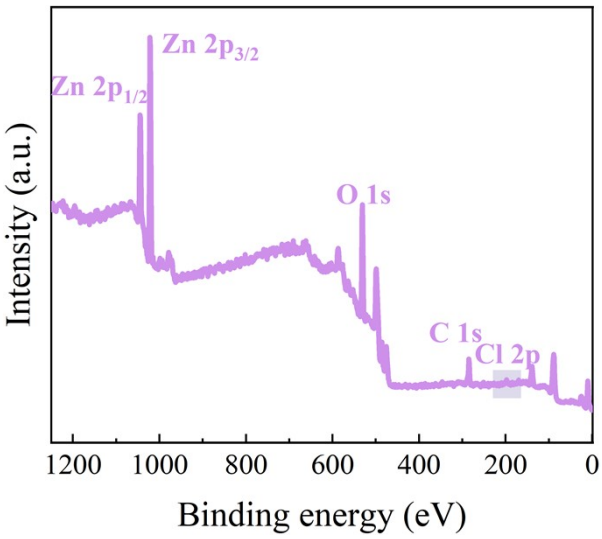

Figure S11. XPS survey spectra of the Zn film in DES5 electrolyte.

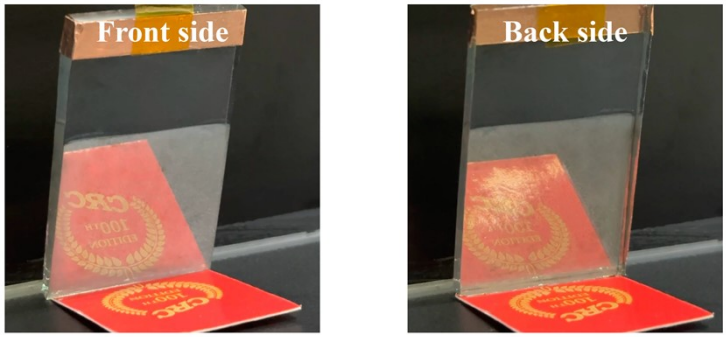

Figure S12. The digital photos of the electrode under front and back sides mirror state.

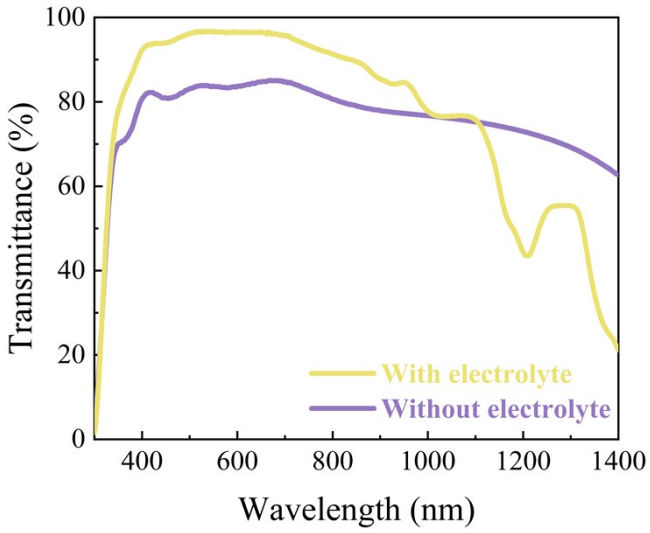

Figure S13. Transmittance spectra of the device with and without electrolyte.

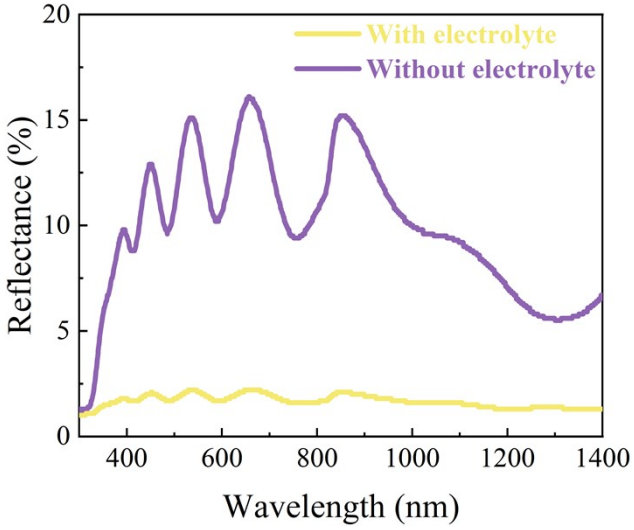

Figure S14. Reflectance spectra of the device with and without electrolyte.

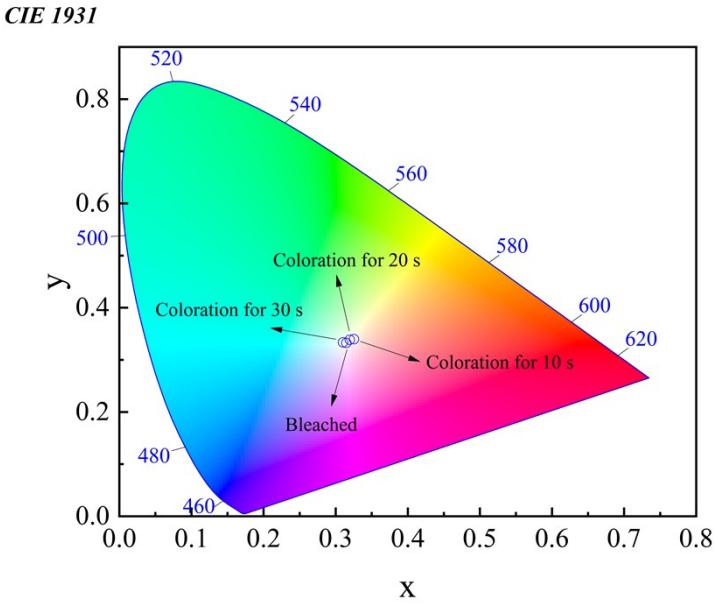

Figure S15. CIE color space and corresponding chromaticity diagram of the device from the transmittance spectra in Figure 5a.

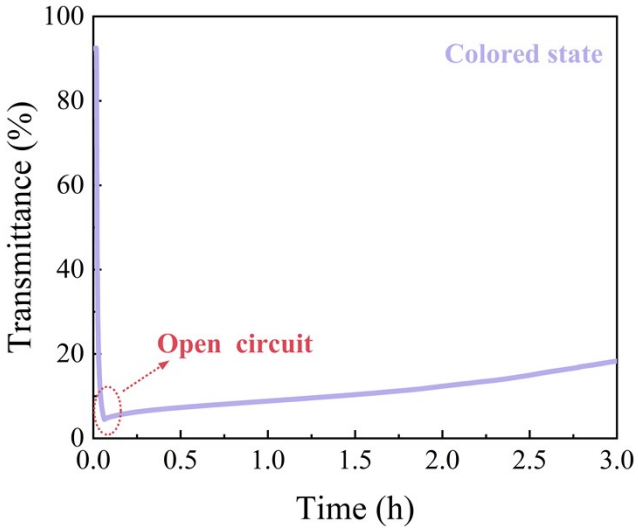

Figure S16. In situ dynamic transmittance spectra at 630 nm of the colored device under open-circuit conditions over 3 h.

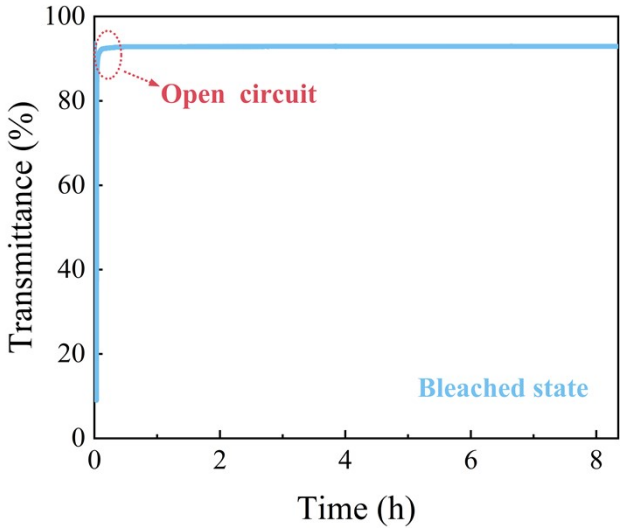

Figure S17. In situ dynamic transmittance spectra at 630 nm of the bleached device under open-circuit conditions over 8 h.

Table S1. Various metal materials and relevant properties as a work electrode material for RME electrochromic devices. Costs are for bulk metals and were found on November 21, 2025 using https://price.metal.com/.

Material	Conductivity (S/m)	Standard reduction potential (V vs. SHE)	Raw cost (CNY/mt)	Inherent color
Cu	5.96×10^7	0.337	8.6×10^4	Reddish brown
Ni	1.43×10^7	-0.25	1.1×10^5	Silvery white
Zn	1.69×10^7	-0.76	2.2×10^4	Silvery white
Bi	7.75×10^5	0.308	1.4×10^5	Silvery white
Pb	4.55×10^6	-0.126	1.7×10^4	Silvery white
Ag	6.30×10^7	0.80	1.2×10^7	Silvery white

Table S2. Properties of our deep eutectic solvent electrolyte and other electrolyte systems.

Ref.	Electrolytes	Voltage window (V)	Ionic conductivity (mS/cm at 20-25 °C)	Operating temperature range (°C)	Appearance
This work	ChCl/EG/$ZnCl_2$	2.7	6.8-8.0	-20~80	Colorless
1	ChCl/urea/LiCl	1.8 (vs. ITO)	0.3	25	Transparent green
2	ChCl/EG/LiTFSI	1.8	8.27	-25~60	Colorless
3	ChCl/glycerol/$CuCl_2$/H_2O	~2 (vs. Ag/AgCl)	0.155	25	Colorless
4	20 mol/kg LiCl/H_2O	2.3 (vs. Ag/AgCl)	60.7	-30~80	Colorless
	1 mol/L LiCl/H_2O	1.7 (vs. Ag/AgCl)	43.2		
5	5 mol/L $Ca(OTF)_2$/H_2O	2 V	12	25	None
	1 mol/L $Ca(OTF)_2$/H_2O	1.38 V	15		
6	KOTF-H_2O	1.32 (vs. Ag/AgCl)	39.43	25	Colorless
	KOTF-PC/H_2O	1.67 (vs. Ag/AgCl)	29.96		
7	LiTFSI/$LiNO_3$/DOL/DME	4 (vs. Li/Li^+)	~10.5	-80~20	None
	LiTFSI/$LiNO_3$/DOL/DME/FEC		~9.5		
	LiTFSI/$LiNO_3$/DOL/DME/EC		~12		
8	LiFSA/DMC (1:10)	~4.4 (vs. Li/Li^+)	9.9	25-40	Colorless
	LiFSA/DMC (1:2)	~5.2 (vs. Li/Li^+)	4.2		
	LiFSA/DMC (1:1.3)	~5.0 (vs. Li/Li^+)	1.7		
	LiFSA/DMC (1.1)	~5.3 (vs. Li/Li^+)	1.1		

Table S3. Nucleation overpotential and mass-transfer overpotential of different DES electrolytes.

Electrolytes	DES1	DES2	DES3	DES4	DES5
Nucleation overpotential	138 mV	117 mV	112 mV	104 mV	104 mV
Mass-transfer overpotential	62 mV	50 mV	48 mV	38 mV	31 mV

Table S4. Color Neutrality of the device in L*a*b Color Space.

States	Luminosity	a	b	$(a^2+b^2)^{1/2}$
Bleached	98.09	-0.82	1.77	1.95
Coloration (10 s)	71.85	0.93	4.99	5.08
Coloration (20 s)	45.36	-0.58	2.59	2.65
Coloration (30 s)	32.04	-1.54	0.52	1.63

Note: The color neutrality was quantitatively assessed by calculating the chroma, defined as $(a^2+b^2)^{1/2}$, from the L*a*b* values. A chroma value of less than 10 is widely considered to represent a neutral color.

Table S5. Memory performance of our DES-based device and other reversible metal electrodeposition devices.

Ref.	Electrolytes	Memory performance (colored state)	Retention $\left(\frac{T_b - T_{c1}}{T_b - T_{c0}}\right)$ (%)
This work	Zn-DES	3 h	84
9	CuZn-DMSO	1 h	~0
3	Cu-DES/aqueous	67 min	~0
10	CuBi-aqueous	10 h	~100
11	ZnMn-aqueous	8 h	~99
12	NiCu-DMSO	>1 h	~0
13	CuSn-DMSO	100 min	~0
14	AgCu-DMSO	2 h	>90*

*estimate value

Table S6. The property comparison of the DES-based device with other reported works.

Ref.	Electrolytes	Transmittance modulation (%)/λ	Reflectance modulation (%)/λ	Operating temperature (°C)	Cyclic stability (cycle)	Switching speed (t_c/t_b, s)
This work	Zn-DES	89/630 nm	23/660 nm	-20~80	2400	30/16
9	CuZn-DMSO	80/550 nm	None	25	1400	120/>50
3	Cu-DES/aqueous	75/550 nm	56/780 nm	25	5000	60/60
10	CuBi-aqueous	>66/600 nm	None	25	1800	15/6.5
11	ZnMn-aqueous	51/633 nm	None	25	100	100/30
12	NiCu-DMSO	55/550 nm	None	20-80	1500	6.2/13.2
13	CuSn-DMSO	79/550 nm	43/730 nm	25	2400	9.8/18.4
15	Zn-DMSO	75/600 nm	52/450 nm	25	2500	30/15
16	Zn-aqueous	80/600 nm	None	30~60	2500	30/30
17	AgCu-NMP/PVB	75/550 nm	None	25	300	87/164
18	Zn-aqueous	80/550 nm	None	25-65	1000	13.5/77

References:

1 K. Rong, H. Zhang, H. Zhang, Y.-Y. Hu, Y. Fang and S. Dong, *Deep Eutectic Solvent with Prussian Blue and Tungsten Oxide for Green and Low-Cost Electrochromic Devices*, *ACS Applied Electronic Materials*, 2019, **1**, 1038-1045.

2 M. Ma, S. Jia, C. Bian, W. Yang, Y. Zhong, J. Ma and G. Cai, *Wide-Temperature Adaptive Electrochromic Device Enabled by Deep Eutectic Solvent-Based Electrolytes*, *Advanced Functional Materials*, DOI: https://doi.org/10.1002/adfm.202520971, e20971.

3 A. L.-S. Eh, J. Chen, X. Zhou, J.-H. Ciou and P. S. Lee, *Robust Trioptical-State Electrochromic Energy Storage Device Enabled by Reversible Metal Electrodeposition*, *ACS Energy Letters*, 2021, **6**, 4328-4335.

4 Y. Chen, Z. Wang, B. Fan, C. Zhang, S. Li, X. Tang, Y. Li, X. Wang, C. Wang, D. Li, S. Cong and Z. Zhao, *Temperature-Tolerant Electrochromic Devices Enabled by LiCl Water-in-Salt Electrolyte with Excellent Performance*, *Chinese Chemical Letters*, 2025, DOI: https://doi.org/10.1016/j.cclet.2025.110824, 110824.

5 Z. Tong, T. Kang, Y. Wan, R. Yang, Y. Wu, D. Shen, S. Liu, Y. Tang and C.-S. Lee, *A Ca-Ion Electrochromic Battery via a Water-in-Salt Electrolyte*, *Advanced Functional Materials*, 2021, **31**, 2104639.

6 W. Zhang, H. Li and A. Y. Elezzabi, *A Dual-Mode Electrochromic Platform Integrating Zinc Anode-Based and Rocking-Chair Electrochromic Devices*, *Advanced Functional Materials*, 2023, **33**, 2300155.

7 A. C. Thenuwara, P. P. Shetty, N. Kondekar, S. E. Sandoval, K. Cavallaro, R. May, C.-T. Yang, L. E. Marbella, Y. Qi and M. T. McDowell, *Efficient Low-Temperature Cycling of Lithium Metal Anodes by Tailoring the Solid-Electrolyte Interphase*, *ACS Energy Letters*, 2020, **5**, 2411-2420.

8 J. Wang, Y. Yamada, K. Sodeyama, C. H. Chiang, Y. Tateyama and A. Yamada, *Superconcentrated Electrolytes for a High-Voltage Lithium-Ion Battery*, *Nature Communications*, 2016, **7**, 12032.

9 D. Zhuang, Z. Zhang, J. Weng, J. Wang, H. Zhang and W. Cheng, *Amorphous Hydrated Tungsten Oxides with Enhanced Pseudocapacitive Contribution for Aqueous Zinc-Ion Electrochromic Energy Storage*, *Advanced Energy Materials*, 2024, **14**, 2402603.

10 Y. Ding, Q. Qiu, Y. Li, J. Shi, L. Du, T. Zhang, X. Liu, C. Li and Z. Li, *Reversible Metal Electrodeposition Enabled by Composites of PEDOT:PSS/MXene for Durable Smart Windows with Broadband Electromagnetic Wave Modulation*, *Small*, 2025, **21**, e06630.

11 H. Palamadathil Kannattil, L. Martinez Soria Gallo, K. D. Harris, B. Limoges and V. Balland, *Innovative Energy Storage Smart Windows Relying on Mild Aqueous Zn/MnO_2 Battery Chemistry*, *Advanced Science*, 2024, **11**, 2402369.

12 X. Guo, J. Chen, A. L.-S. Eh, W. C. Poh, F. Jiang, F. Jiang, J. Chen and P. S. Lee, *Heat-Insulating Black Electrochromic Device Enabled by Reversible Nickel-Copper Electrodeposition*, *ACS Applied Materials & Interfaces*, 2022, **14**, 20237-20246.

13 A. L.-S. Eh, J. Chen, S. H. Yu, G. Thangavel, X. Zhou, G. Cai, S. Li, D. H. C. Chua and P. S. Lee, *A Quasi-Solid-State Tristate Reversible Electrochemical Mirror Device with Enhanced Stability*, *Advanced Science*, 2020, **7**, 1903198.

14 C. Park, S. Seo, H. Shin, B. D. Sarwade, J. Na and E. Kim, *Switchable Silver Mirrors with Long Memory Effects*, *Chemical Science*, 2015, **6**, 596-602.

15 N. C. Bhoumik, D. C. Madu, C. W. Moon, L. S. Arvisu, M. D. McGehee and C. J. Barile, *Nonaqueous Electrolytes for Reversible Zinc Electrodeposition for Dynamic Windows with Excellent Optical Contrast and Durability*, *Joule*, 2024, **8**, 1036-1049.

16 S. M. Islam and C. J. Barile, *Dynamic Windows Using Reversible Zinc Electrodeposition in Neutral Electrolytes with High Opacity and Excellent Resting Stability*, *Advanced Energy Materials*, 2021, **11**, 2100417.

17 Z. Li, L. Yuan and X. Yang, *Dynamic Color Display with Tuneable Gamut by Surface Resistance Control in ITO-Based Electrochromic Devices*, *Solar Energy Materials and Solar Cells*, 2025, **290**, 113720.

18 K. Wang, F. Zhang, X. Jiang, W. Zhang, L. Dai, J. Zhang, Z. Li and H. Jia, *Bionic Nanogel Interfaces Unlock Long-Term Stability in Zn Metal Electrodeposition-Based Electrochromic Windows*, *Advanced Materials*, 2025, **37**, e09980.